Theoretical Studies of Inorganic and Organometallic Reaction Mechanisms. 6. Methane Activation on Transient Cyclopentadienylcarbonylrhodium

Jun Song and Michael B. Hall*

Department of Chemistry, Texas A&M University, College Station, Texas 77843-3255

Received May 13, 1993

The C-H oxidative-addition of methane to the transient RhCp(CO) complex was studied with ab initio RHF and MP2 techniques. Electron correlation dramatically alters the reaction energetics and shifts the intermediate later and the transition state earlier in the reaction coordinate. The MP2 calculations predict an intermediate stabilized by 14.8 kcal/mol, a transition state with an activation barrier of 4.1 kcal/mol relative to the intermediate, and a reaction product exothermic by 30.6 kcal/mol. Analyses of the molecular structure and the Laplacian of the total charge density reveal an agostic-like intermediate with metal-CH dative interaction in the early stage of the reaction. The transition state shows obvious C-H bond breaking and is significantly stabilized by newly forming Rh-C and Rh-H bonding interactions.

Introduction

Carbon-hydrogen activation will be the most fundamental step in any catalytic cycle designed to convert vast methane sources into useful products. In contrast to H-H activation, relatively few transition metal complexes break "unactivated" C-H bonds of alkanes. Ever since the successful activation of alkyl C-H bonds by rhodium and iridium complexes in 1982,[1] the elucidation of the reaction mechanism has attracted both experimental[2] and theoretical[3] interest.

Basically, the mechanism is an oxidative-addition reaction, in which a metal center inserts into the C-H linkage of the alkane, R-H, as shown in eq 1. For

$$M + R\text{-}H \rightarrow R\text{-}M\text{-}H \qquad (1)$$

unsaturated transition metal complexes, the early stages of C-H oxidative-addition may involve coordination of the C-H bond itself to the metal and lead to the formation of an intermediate. First discovered in 1974,[4] these M···H-C systems are in more recent work referred to as "σ-complexes",[5] "alkane complexes",[6] or "agostic complexes"[5] by other research groups.

Recently, Wasserman, Moore, and Bergman directly measured the rates of reactions between the transient 16-electron complex, CpRh(CO), and alkanes in the gas phase.[8] On the basis of these new experimental results and previous investigations, they proposed the following reaction sequence[8] which involves formation of an intermediate:

$$\underset{\text{reactant}}{RH} + RhCp(CO) \rightarrow \underset{\text{intermediate}}{RH\text{- - -}RhCp(CO)} \rightarrow \underset{\text{product}}{RHRhCp(CO)} \qquad (2)$$

These authors estimated the bond energy between the RhCp(CO) complex and the alkane in the intermediate to be about 10 kcal/mol, a value which is much larger than that expected from van der Waals forces alone. From the intermediate to the transition state, the measured barrier is 4.5 kcal/mol for both cyclohexane and neopentane.

These novel experiments are very important to the development of carbon-hydrogen activation chemistry. However, since the reactions proceed very rapidly, the assumed intermediate was not detected in the experiments.[8] Thus, details about the nature of the intermediate, especially its structure remain unknown.

In this work, we investigated the important features of reaction 2 by using CH_4 as a model alkane. Along the reaction coordinate, we calculated the geometries, energetics, and electron density distributions in detail. The

(1) (a) Janowicz, A. H.; Bergman, R. G. *J. Am. Chem. Soc.* **1982**, *104*, 352. (b) Crabtree, R. H.; Mellea, M. F.; Mihelcie, J. M.; Quick, J. M. *J. Am. Chem. Soc.* **1982**, *104*, 107. (c) Hoyano, J. K.; Graham, W. A. G. *J. Am. Chem. Soc.* **1982**, *104*, 3723. (d) Jones, W. D.; Feher, F. J. *J. Am. Chem. Soc.* **1982**, *104*, 4240.

(2) For reviews, see: (a) Muetterties, E. L. *Chem. Soc. Rev.* **1983**, *12*, 283. (b) Shilov, A. E. *Activation of Saturated Hydrocarbons by Transition Metal Complexes*; Reidel: Dordrecht, Holland, 1984. (c) Bergman, R. G. *Science*, **1984**, *223*, 902. (d) Crabtree, R. H. *Chem. Rev.* **1985**, *85*, 245-269. (e) Halpern, J. *Inorg. Chim. Acta* **1985**, *100*, 41. (f) Jones, W. D.; Feher, F. J. *Acc. Chem. Res.* **1989**, *22*, 91. (g) Ryabov, A. D. *Chem. Rev.* **1990**, *90*, 403.

(3) (a) Noell, J. O.; Hay, P. J. *J. Am. Chem. Soc.* **1982**, *104*, 4578. (b) Blomberg, M. R. A.; Brandemark, U.; Siegbahn, P. E. M. *J. Am. Chem. Soc.* **1983**, *105*, 5557. (c) Saillard, J.-Y.; Hoffmann, R. *J. Am. Chem. Soc.* **1984**, *106*, 2006. (d) Low, J. J.; Goddard, W. A., III. *J. Am. Chem. Soc.* **1984**, *106*, 6928; **1986**, *108*, 6115. (e) Obara, S.; Kitaura, K.; Morokuma, K. *J. Am. Chem. Soc.* **1984**, *106*, 7482. (f) Rabaa, H.; Saillard, J.-Y.; Hoffmann, R. *J. Am. Chem. Soc.* **1986**, *108*, 4327. (g) Anderson, A. B.; Baldwin, S. *Organometallics* **1987**, *6*, 1621. (h) Ziegler, T.; Tschike, V.; Fan, L.; Becke, A. D. *J. Am. Chem. Soc.* **1989**, *111*, 9177. (i) Blomberg, M. R. A.; Schule, J.; Siegbahn, P. E. M. *J. Am. Chem. Soc.* **1989**, *111*, 6156. (j) Koga, N.; Morokuma, K. *J. Phys. Chem.* **1990**, *94*, 5454. (k) Blomberg, M. R. A.; Siegbahn, P. E. M.; Nagashima, U.; Wennerberg, J. *J. Am. Chem. Soc.* **1991**, *113*, 424. (l) Blomberg, M. R. A.; Siegbahn, P. E. M.; Svensson, M. *New. J. Chem.* **1991**, *15*, 727. (m) Hay, P. J. *Transition Metal Hydrides*; Dedieu, A., Ed.; VCH Publishers: New York, 1992 and references therein.

(4) (a) Cotton, F. A.; LaCour, T.; Stanislowski, A. G. *J. Am. Chem. Soc.* **1974**, *96*, 754. (b) Cotton, F. A.; Stanislowski, A. G. *J. Am. Chem. Soc.* **1974**, *96*, 5074. (c) Cotton, F. A.; Day, V. W. *J. Chem. Soc., Chem. Commun.* **1972**, 415. (d) Cotton, F. A.; Luck, R. L. *Inorg. Chem.* **1989**, *28*, 3210.

(5) (a) Periana, R. A.; Bergman, R. G. *J. Am. Chem. Soc.* **1986**, *108*, 7332. (b) Bullock, R. M.; Headford, C. E. L.; Hennessy, K. M.; Kegley, S. E.; Norton, J. R. *Ibid.* **1989**, *111*, 3897.

(6) Kafafi, Z. H.; Hauge, R. H.; Margrave, J. L. *J. Am. Chem. Soc.* **1985**, *107*, 6134.

(7) For reviews, see: (a) Brookhart, M.; Green, M. L. H. *J. Organomet. Chem.* **1983**, *250*, 395. (b) Crabtree, R. H. *Chem. Rev.* **1985**, *85*, 245. (c) Brookhart, M.; Green, M. L. H.; Wong, L.-L. *Prog. Inorg. Chem.* **1988**, *36*, 1-124. (d) Crabtree, R. H.; Hamilton, D. G. *Adv. Organomet. Chem.* **1988**, *28*, 299.

(8) (a) Wasserman, E. P.; Moore, C. B.; Bergman, R. G. *Science* **1992**, *255*, 315. (b) Weiller, B. H.; Wasserman, E. P.; Bergman, R. G.; Moore, C. B.; Pimentel, G. C. *J. Am. Chem. Soc.* **1989**, *111*, 8288.

0276-7333/93/2312-3118$04.00/0

results predict that oxidative-addition of CH_4 to RhCp(CO) proceeds through an agostic-like intermediate. With a perturbation-theory correlation correction (MP2), the calculated energetics are in agreement with the experimental results.

Calculational Details

The core electrons of Rh were fitted to an effective core potential where the 4s and 4p electrons are treated explicitly as valence electrons of the Rh atom (ECP 2). The valence electrons were described with the double-ζ basis (541/41/31) of Hay and Wadt.[9a] For carbon and oxygen, effective core potentials and basis sets of Stevens, Basch, and Krauss[9b] were used in a double-ζ form. The basis set of hydrogen was a double-ζ (21) contraction.[10] Our previous work on the oxidative-addition of H_2 to Ir suggests that this basis set is adequate.[11]

Ab initio calculations were carried out via the restricted Hartree–Fock (RHF) methods.[12] Full-gradient techniques were utilized for geometry optimization calculations. Electron correlation was considered at the second-order Møller–Plesset (MP2) level.[13] Again, our previous work supports the adequacy of the MP2 level of calculation for oxidative addition reactions such as this one.[11]

All the RHF geometry optimizations were performed with the GAMESS package[14] at the Cornell National Supercomputer Facility on an IBM 3090-600VF, at the Supercomputer Center of Texas A&M University on a Cray Y-MP2/116, and at the Chemistry Department on a FPS Model 522. All the MP2 calculations were carried out by using the GAUSSIAN 90 program[15] at the Cornell National Supercomputer. The topological analysis of the total charge density was performed with the use of Bader's theory,[16] which has been incorporated into the MOPLOT program.[17]

The following restrictions have been utilized to simplify the geometry optimizations along the reaction coordinate. For the reaction system 1, the RhCp fragment was fixed to have local C_{5v} symmetry with a planar Cp ring. The Rh–C–O angle was constrained to be linear. The C–C and C–H distances in the Cp ring were set to 1.411 and 1.080 Å, respectively, values typical for metal-bound C_5H_5. The spectator CH_3 fragment of the methane was treated as a C_{3v} fragment with tetrahedral angles and a C–H bond length of 1.094 Å, which is the optimized C–H bond length in methane at the RHF level in our basis. One of the spectator hydrogen atoms in CH_3 fragment, H′, was restricted to remain in the Rh–H–C plane as shown in 1. This later constraint was necessary because the CH_3 has nearly free rotation for much of the reaction path. All of the other geometric parameters were allowed to change in the optimization. Thus we maintained C_s symmetry throughout the reaction path.

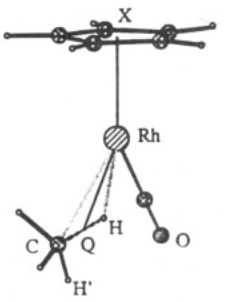

1

Results and Discussion

A. Potential Energy Curves. For a given reaction system, the variations in energy and molecular geometry generally can be predicted by following a reaction path from reactant to product. However, in large systems it is difficult and time consuming to find the true reaction path. An approximate path is often generated by constructing a potential energy curve or surface, which is obtained through fixing one or two of the internal coordinates at successive values while optimizing all the other geometric parameters.

First, we calculated the potential energy curve at the RHF level by optimizing the geometries of 1 along the coordinate R_{Rh-Q}, where Q is the center of the activated C–H bond. The upper curve in Figure 1 presents the calculated results. For the optimization of the reactants, we set the R_{Rh-Q} distance to 6.0 Å, a value large enough that the geometry of CH_4 in this system is almost the same as that of a free CH_4 at the same theoretical level. As R_{Rh-Q} decreased, two local energy minima occurred on the RHF potential energy curve (see Figure 1). The early minimum corresponds to the reaction intermediate, while the late one corresponds to the oxidative-addition product.

In the transition state region (around R_{Rh-Q} = 1.70 Å), we found discontinuities in other geometric parameters and in the dipole moment. This observation usually implies that the assumed reaction coordinate is a poor representation of the true reaction coordinate.[18] To clarify this problem, we constructed a potential energy surface on coordinates R_{Rh-Q} and R_{C-H}. Figure 2 shows the contour plot of the potential energy surface. In the area of the saddle point b, as shown in Figure 2, the energy contour lines are almost parallel to coordinate R_{C-H} (or R_{Rh-Q}). Therefore, the one-coordinate optimization procedure may lead to a range of geometries which have the same energy and R_{Rh-Q} (or R_{C-H}), but have different R_{C-H} (or R_{Rh-Q}). To make up for the deficiency of the one-coordinate procedure, we used the energies and optimized geometries of points c, b, and a to characterize the RHF reaction path in the transition-state region.

Although the RHF optimization predicts a reaction intermediate, as demonstrated in Table I, the RHF calculations suggest an unfavorable reaction both thermodynamically and kinetically. The endothermicity and activation barrier are 19.8 and 31.4 kcal/mol, respectively. These results obviously contradict the experimental findings.[7] Therefore, we examined the reaction at a higher theoretical level. Since the second-order Møller–Plesset (MP2) perturbation method provided a reliable prediction

(9) (a) Hay, P. J.; Wadt, W. R. *J. Chem. Phys.* **1985**, *82*, 270. (b) Stevens, W. J.; Basch, H.; Krauss, M. *J. Chem. Phys.* **1984**, *81*, 6026.
(10) Hehre, W. J.; Stewart, R. F.; Pople, J. A. *J. Chem. Phys.* **1969**, *51*, 2657.
(11) Lin, Z.; Hall, M. B. *J. Am. Chem. Soc.* **1992**, *114*, 2928.
(12) (a) Roothaan, C. C. J. *Rev. Mod. Phys.* **1951**, *23*, 69. (b) Roothaan, C. C. *J. Rev. Mod. Phys.* **1960**, *32*, 179.
(13) (a) Møller, C.; Plesset, M. S. *Phys. Rev.* **1936**, *46*, 618. (b) Pople, J. A.; Binkley, J. S.; Seeger, R. Int. *J. Quantum Chem.* **1976**, *S10*, 1.
(14) Guest, M. F., SERC Daresbury Laboratory, Warrington WA4 4AD, U.K.
(15) Frisch, M. J.; Head-Gordon, M.; Trucks, G. W.; Foresman, J. B.; Schlegel, H. B.; Raghavachari, K.; Robb, M.; Binkley, J. S.; Gonzalez, C.; Defrees, D. J.; Fox, D. J.; Whiteside, R. A.; Seeger, R.; Melius, C. F.; Baker, J.; Martin, R. L.; Kahn, L. R.; Stewart, J. J. P.; Topiol, S.; Pople, J. A. Gaussian, Inc., Pittsburgh, PA, 1990.
(16) (a) Bader, R. F. W.; Essen, H. *J. Chem. Phys.* **1984**, *80*, 1943. (b) Bader, R. F. W.; MacDougall, P. J.; Lau, C. D. H. *J. Am. Chem. Soc.* **1984**, *106*, 1594.
(17) Interactive MOPLOT: a package for the interactive display and analysis of molecular wavefunctions incorporating the program MOPLOT (Lichtenbruger, D.), PLOTDEN (Bader, R. F. W.; Kenworthy, D. J.; Beddal, P. M.; Runtz, G. R.; Anderson, S. G.), SCHUSS (Bader, R. F. W.; Runtz, G. R.; Anderson, S. G.; Biegler-Koenig, F. W.) and EXTREM (Bader, R. F. W.; Biegler-Koenig, F. W.); Sherwood, P.; MacDougall, P. J., 1989.
(18) (a) Ishida, K.; Morokuma, K.; Komornicki, A. *J. Chem. Phys.* **1977**, *66*, 2153. (b) Sargent, A. L.; Hall, M. B.; Guest, M. F. *J. Am. Chem. Soc.* **1992**, *114*, 517.

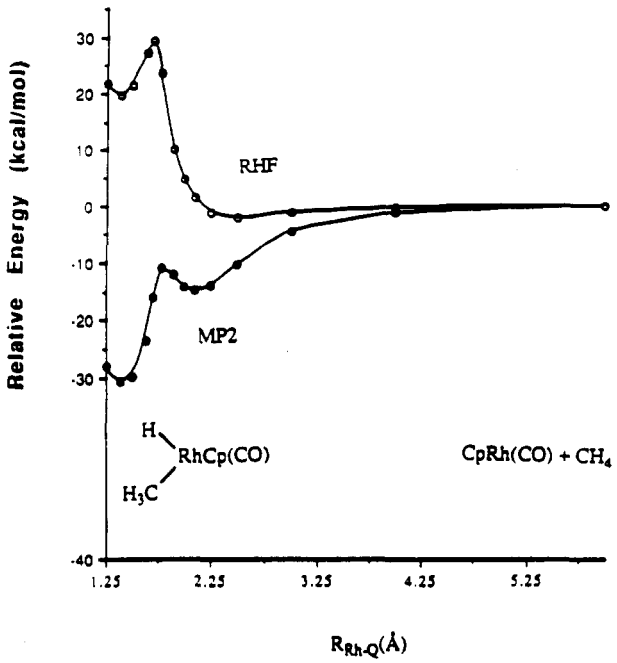

Figure 1. Potential energy curves for the oxidative addition of CH_4 to RhCp(CO) along the coordinate R_{Rh-Q} at the RHF and MP2 levels.

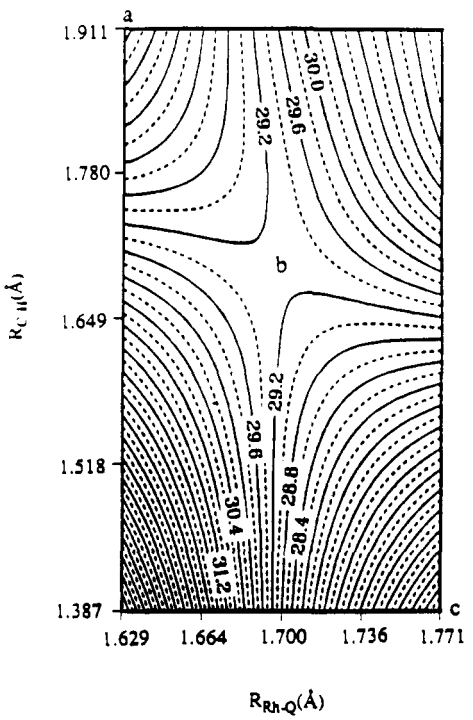

Figure 2. Contour plot of the potential energy surface around the RHF transition state (point b). The energies are in kcal/mol relative to the reactant. The MP2 transition state is very close to point c.

for the relative stability of transition metal hydrides versus dihydrogen complexes[11] and for the potential energy curves of C–H activation by a 14-electron complex, $RhCl(PH_3)_2$,[3j] we performed MP2 calculations at each of the RHF optimized geometries. Although the corrections from the RHF to the MP2 are large, higher order calculations (MP3, MP4) would not significantly alter our conclusions.[11]

The lower curve in Figure 1 presents the MP2 results. Note the dramatic change in the reaction energetics, a change which shifts the location of the intermediate later and that of the transition state earlier in the reaction profile. As shown in Table I, the MP2 calculations predict the reaction to be exothermic by 30.6 kcal/mol. An intermediate is also clearly observable early in the reaction with a stabilization energy of 14.8 kcal/mol. The activation energy with respect to the intermediate is 4.1 kcal/mol. All of these energy features, especially the activation barrier, are in good agreement with the experimental results (see Table I). Thus, the MP2 calculations provide an adequate theoretical level for further investigations of molecular geometries, electronic structures, and kinetic features of the reaction.

Table I. Reaction Energy, ΔH, Stabilized Energy of the Intermediate, ΔE_{int}, and Activation Barrier, ΔE_{act}, for the Addition of CH_4 to RhCp(CO)

	ΔH (kcal/mol)	ΔE_{int}[a] (kcal/mol)	ΔE_{act}[b] (kcal/mol)
RHF	19.8	-2.2	31.4
MP2	-30.6	-14.8	4.1
experiment[c]	<-15	~-10	4.5

[a] I.e. the energy of the intermediate relative to the reactant. [b] The barrier from the intermediate to transition state. [c] Reference 8.

B. Electron Correlation Effects. The marked difference between the RHF and MP2 energy profiles shows the importance of electron correlation in this reaction system. The reasons behind this dramatic effect is the inability of the Hartree–Fock method to describe the Rh–C and Rh–H bonds as well as it describes the C–H bond. Since the size of the rhodium is much larger than that of the carbon or hydrogen, the orbitals of the rhodium do not overlap the orbitals of the carbon or hydrogen as well as these orbitals overlap each other. As a result, the Rh–C and Rh–H bonding interactions are underestimated by the RHF method more than the C–H interaction. This problem leads to the unreasonable endothermic reaction profile seen above. (For additional insight, see ref 19.)

If these analyses are correct, the electron correlation effect should gradually become increasingly stronger from the reactant to the product. Indeed, we observed this tendency in the upper curve of Figure 3, which shows the change in the energy difference between the MP2 and RHF results along the coordinate R_{Rh-Q}. For comparison, we plotted the corresponding values of the C–H distance as shown in the lower curve of Figure 3. Note the rapidly increasing electron correlation effect in the late stage of the reaction. This strong effect is absent in the early stage because the C–H bonding interaction is still very important here.

C. Important Molecular Structures. Figure 4 shows the molecular structures of the reactant, intermediate, transition state, and product along the MP2 curve (see Figure 1). As mentioned above, the MP2 calculations have shifted the intermediate later and the transition state earlier. Since the MP2 intermediate is close to R_{Rh-Q} = 2.1 Å, where the RHF geometry optimization has been performed, we take the RHF geometry of 2.1 Å as the structure of the MP2 intermediate. Likewise, we use the RHF optimized geometry of the point c in Figure 2 as the structure of the MP2 transition state.

The electronic structure of RhCp(CO), a coordinatively unsaturated complex, has attracted theoretical interest.[3h,20] Our calculations suggested that this 16-electron system has a X–Rh–C_o angle of 137.2°, where X is the center of

(19) Low, J. J.; Goddard, W. A., III. *J. Am. Chem. Soc.* **1986**, *108*, 6115.
(20) Hofmann, P.; Padmanabhan, M. *Organometallics* **1983**, *2*, 1273.

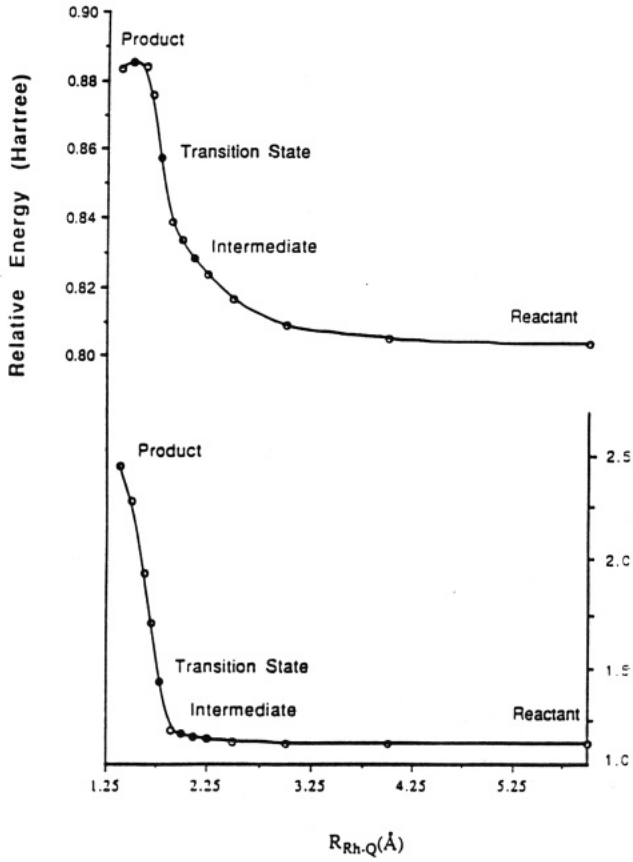

Figure 3. Variations of ΔE (the difference between the MP2 and RHF energies) and R_{C-H} (the C–H distance) from the reactant to product. The intermediate or transition state is denoted by ●.

the Cp ring and C_o is the carbon of the CO ligand. Both the singlet and triplet state have a similar bent geometry and at the MP2 level are nearly degenerate.

As shown in Figure 4, our optimizations predict an intermediate with a bent Rh–H–C_{H3} geometry (angle Rh–H–C_{H3} = 114.9°). As expected, the C–H bond distance in the intermediate (1.128 Å) is slightly longer than that in the reaction (1.094 Å). The Rh–H and Rh–C distances are calculated to be 1.799 and 2.494 Å, respectively. Interestingly, the geometry of Rh–H–C in the intermediate is similar to that in [RhCp*(C_6H_{11})][BF_4], an agostic compound recently characterized by X-ray studies.[21] As shown in Table II, both the Rh–H and C–H distances in the intermediate are close to those in the RhCp*(C_6H_{11}) complex (R_{Rh-H} = 1.88 Å, R_{C-H} = 1.12 Å) although the angle Rh–H–C in the intermediate (114.9°) is larger than that in the RhCp*(C_6H_{11}) complex (99°) by 15.9°. However, since this bond angle decreased by 10.8° from the RHF intermediate to the MP2 intermediate, a complete geometry optimization at the MP2 level may further decrease the Rh–H–C bond angle. On the other hand, the bonding of the rest of the C_6H_{11} fragment to the Rh may constrain the Rh–H–C angle in the RhCp*(C_6H_{11}) complex.

From Figure 3, we have seen that a marked elongation (0.259 Å) of the C–H bond occurs from the intermediate to the transition state, which has a C–H distance of 1.387 Å. Thus, the energy increase in the transition state is primarily due to the breaking of the C–H bond. Comparing the molecular structure of the transition state with that

(21) Salzer, A.; Buchmann, B.; Schmalle, H. *Acta Crystallogr.* **1991**, *C47*, 275.

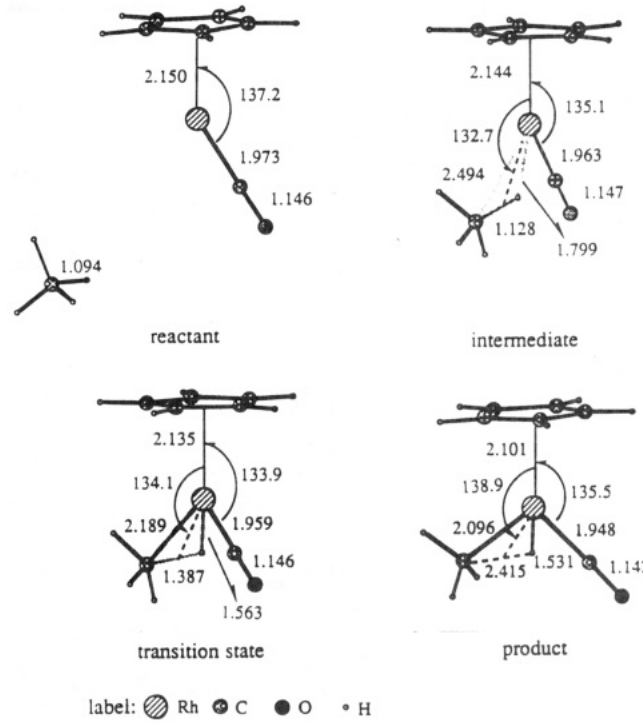

Figure 4. Optimized molecular geometries at the reactant, intermediate, transition state, and product. The important structural parameters are shown in angstroms for bond distances and in degrees for bond angles. These geometries are for the MP2 curve shown in Figure 1.

Table II. Comparison of the Structural Data for the Rh-H-C Fragments in Our Intermediate and an Agostic Compound [RhCp*(C_6H_{11})][BF_4]

	R_{Rh-H} (Å)	R_{C-H} (Å)	Rh-H-C (deg)
intermediate[a]	1.799	1.128	114.9
RhCp*(C_6H_{11})[b]	1.88	1.12	99

[a] This work. [b] Reference 20.

of the product, we observe that in the late stage of the reaction (from the transition state to the product) the Rh–C and Rh–H distances are only shortened by 0.093 and 0.032 Å, respectively. The magnitude of these remaining structural changes suggests that significant Rh–C and Rh–H bonding interactions have formed already in the transition state. The Rh–C and Rh–H bonding interactions in the transition state have stabilized the reaction system and reduced the activation barrier. In the late stage of the reaction, the most obvious geometry variation is the final elongation of the C–H distance (by 1.028 Å), until a stable 18-electron molecular structure is generated in the product.

D. Laplacian of the Total Charge Density. A detailed examination of the Laplacian of the charge density can provide crucial information to understand the process of bond making and breaking during the reaction. Figure 5 shows six Laplacian maps at significant stages along the MP2 reaction path (see Figure 1). The wave functions used to plot these Laplacian maps are the correponding RHF wave functions. Although the MP2 energy corrections are large, the RHF wave function dominates the total wave function throughout the reaction. Thus, we would expect the RHF density (a one-electron property) to be fairly accurate. All Laplacian maps are plotted in the Rh–H–C plane. The plots of the negative of the Laplacian of the charge density, $-\nabla^2\rho$, display regions of local charge concentration ($-\nabla^2\rho > 0$, denoted by solid contours) and

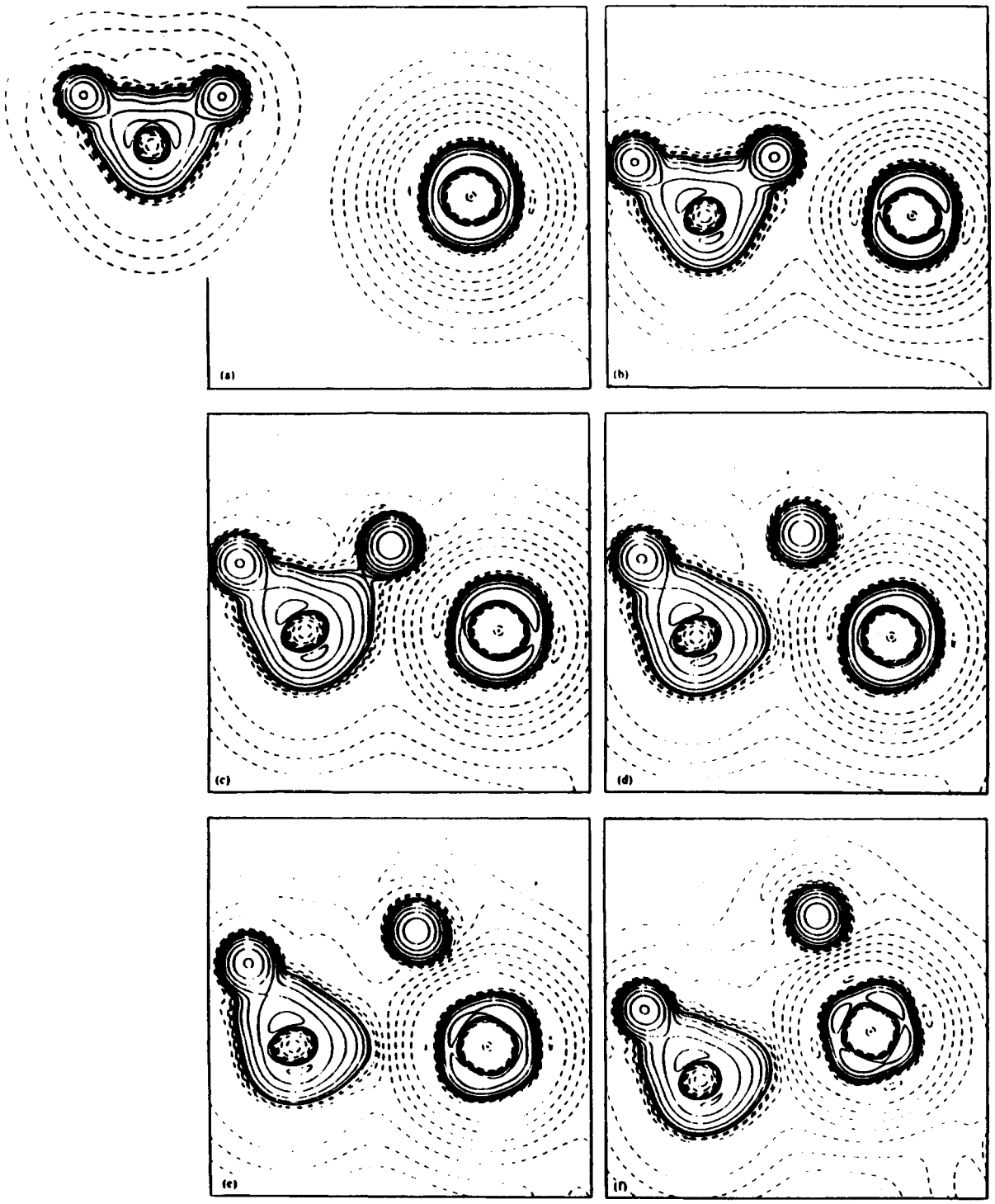

Figure 5. Plots of $-\nabla^2\rho$ for six points along the coordinate R_{Rh-Q}: (a) reactant; (b) intermediate; (c) transition state; (d, e) two points in the late stage; (f) product. The plots are in the Rh–H–C plane, the symmetry plane. CH_4 enters from the left, and the breaking C–H bond is the one approaching Rh (the far atom on the right). Ten geometric contours of each sign are plotted. The absolute value of the smallest contour is 0.66875 e/a_0^5.

of local charge depletion ($-\nabla^2 \rho < 0$, denoted by dashed contours). The evolution of these regions of charge concentration and depletion as the reaction proceeds can provide valuable insight into the overall electronic structure.

For the reactant, Figure 5a, there is no significant interaction between CH_4 and RhCp(CO). The charge concentration around the Rh atom is the contribution from the nonbonded 4d valence electrons in the Rh–H–C plane. The maximum located near the carbon on the C–H linkage line corresponds to a strong C–H bonded concentration.

As the reaction system evolves to the intermediate, Figure 5b, the charge concentration in the Rh valence shell clearly splits into two parts. Meanwhile, the maximum between the C and H moves away from the C–H bond path and decreases its extent. As a result, the C–H bonding interaction is significantly weakened, which is observable by comparing the electron distribution of the activated C–H bond and that of the spectator one.

A depletion, such as the one found between the Rh and C–H bond in the intermediate, usually indicates a dative bond, in which the C–H electron concentration is aligned

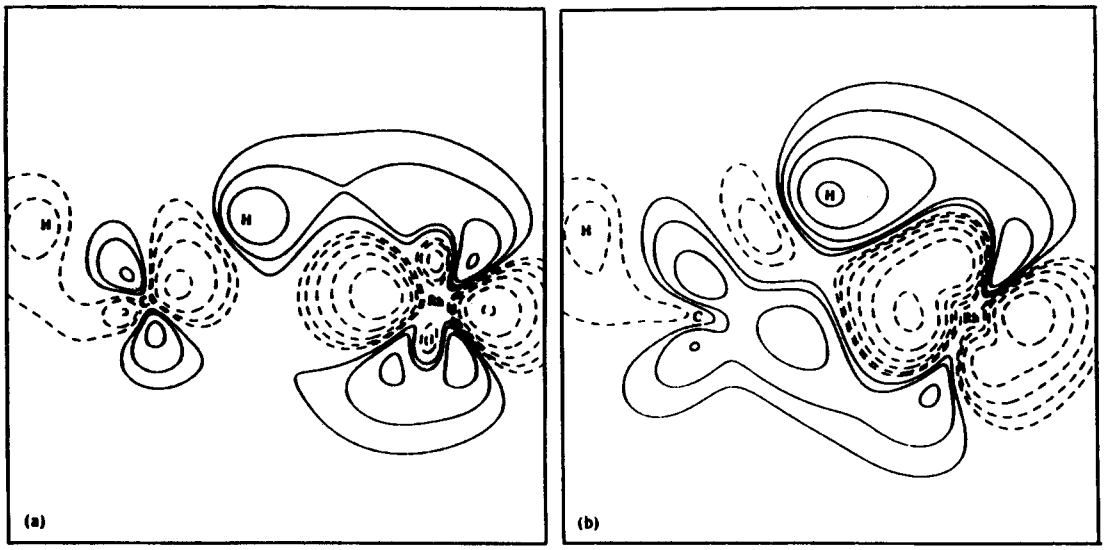

Figure 6. Plots of deformation density for the (a) intermediate and (b) transition state. The plots are obtained by subtracting the electron densities of the promolecules (CH_4 and RhCp(CO)) from the total density of the molecule. The plots are in the Rh–H–C plane. Adjacent lines differ by a factor of 2. The lowest contour is 0.00195 e/au^3.

with (donated to) the hole (vacant site) on the Rh atom. In order to clarify this, we examined the deformation density map of the intermediate (see Figure 6a). Here, the deformation density is the difference between the total density of the intermediate and the densities of the promolecule made from the sums of the densities of CH_4 and RhCp(CO). In addition, we also plotted the deformation density map of the transition state (Figure 6b). Both the maps in Figure 6 are in the Rh–H–C plane.

Figure 6a clearly shows a dative interaction because the largest change is the creation of a hole in Rh in the direction of the C–H bond as the Rh atom prepares a vacant site for the C–H donor. The plot also shows the beginning of the electron transfer (oxidative-addition) process. These donated electrons are primarily transferred to the region between the Rh and H atoms as well as the region between the Rh and C atoms, while there is some loss of C–H bond density. Particularly, the connection of the electron density in the area between the Rh and H atoms suggests the formation of a significant Rh–H bonding interaction. There are also significant internal rearrangements of density on the Rh. Dative interactions between the C–H bonds and metals have been observed in agostic complexes and investigated by molecular orbital analyses in detail.[22]

The Laplacian map of the transition state shows an obvious C–H breaking (see Figure 5c). On the other hand, since both the C and H atoms are close to the Rh atom, Rh–C and Rh–H bond making interactions are also beginning but are less obvious in Figure 5c. These latter interactions as well as the remaining dative bond features are visible in Figure 6b. As demonstrated in Figure 6b, more electrons accumulate between the Rh and H atoms and between the Rh and C atoms. This three-center interaction helps to stabilize the transition state, thus decreasing the activation barrier.

Mulliken population analysis on the fragment orbitals reveals that the net electron distribution of the transition state primarily results from the electron interchange between the frontier orbitals of the CH_4 and RhCpCO fragments. Figure 7 shows the contour plots of the frontier orbitals (RHF calculations) of the CH_4 and RhCpCO fragments in the Rh–H–C plane. The HOMO and LUMO of the CH_4 fragment are the C–H σ bonding orbital (Figure 7a) and σ^* antibonding orbital (Figure 7b), respectively. For the RhCpCO fragment, the HOMO (Figure 7b′) derives from Rh d_π orbital and contains the Rh–Cp antibonding character, while the LUMO (Figure 7a′) mainly derives from Rh 5s orbital. The C–H σ orbital overlapping with the LUMO of RhCpCO fragment leads to electron donation. On the other hand, the C–H σ^* orbital overlapping with the HOMO of RhCpCO fragment induces electron back-donation. Both the electron donation and back-donation aid to break the C–H bond and form the Rh–C and Rh–H bonds.

In the late stage of the reaction, the CH_4 fragment has been separated into two parts. As the H atom and the CH_3 fragment adjust their positions relative to the metal, the electron density of the Rh atom undergoes a corresponding redistribution. This evolution is observed in Figure 5c–e. In Figure 5f, the electron density distribution has evolved into the final stable structure, where the H atom and CH_3 fragment have strongly bonded to the Rh atom through two of the depletions around metal center. This electronic structure is typical of dative and polar covalent bonds in a 6-coordinate d^6 complex,[23] where the metal concentrations are form the nonbonding d orbitals. Since the M–X bond pairs are more concentrated on the ligand (X), a depletion appears on the metal at the site of the M–X bond.

E. A Theoretical Trajectory. Using Burgi–Dunitz's method,[24] Crabtree et al. constructed a C–H + M → C–M–H reaction coordinate from a range of structures of static complexes containing agostic C–H interactions.[25] In this approach, a measure of the C–H bond to metal distance (r_{bp}), the C–H distance (d_{CH}), and the Rh–H–C angle have been compared to help understand the process of C–H activation. It is interesting to compare this

(22) (a) Koga, N.; Obara, S.; Kitaura, K.; Morokuma, K. *J. Am. Chem. Soc.* **1985**, *107*, 7109. (b) Koga, N.; Obara, S.; Kitaura, K.; Morokuma, K. *J. Am. Chem. Soc.* **1984**, *106*, 4625. (c) Eisenstein, O.; Jean, Y. *J. Am. Chem. Soc.* **1985**, *107*, 1177.

(23) MacDougall, P. J.; Hall, M. B. *Trans. Am. Crystallogr. Assoc.* **1990**, *26*, 101.

(24) Burgi, H. B.; Dunitz, J. D. *Acc. Chem. Res.* **1983**, *16*, 153.

(25) Crabtree, R. H.; Holt, E. M.; Lavin, M.; Morehouse, S. M. *Inorg. Chem.* **1985**, *24*, 1986.

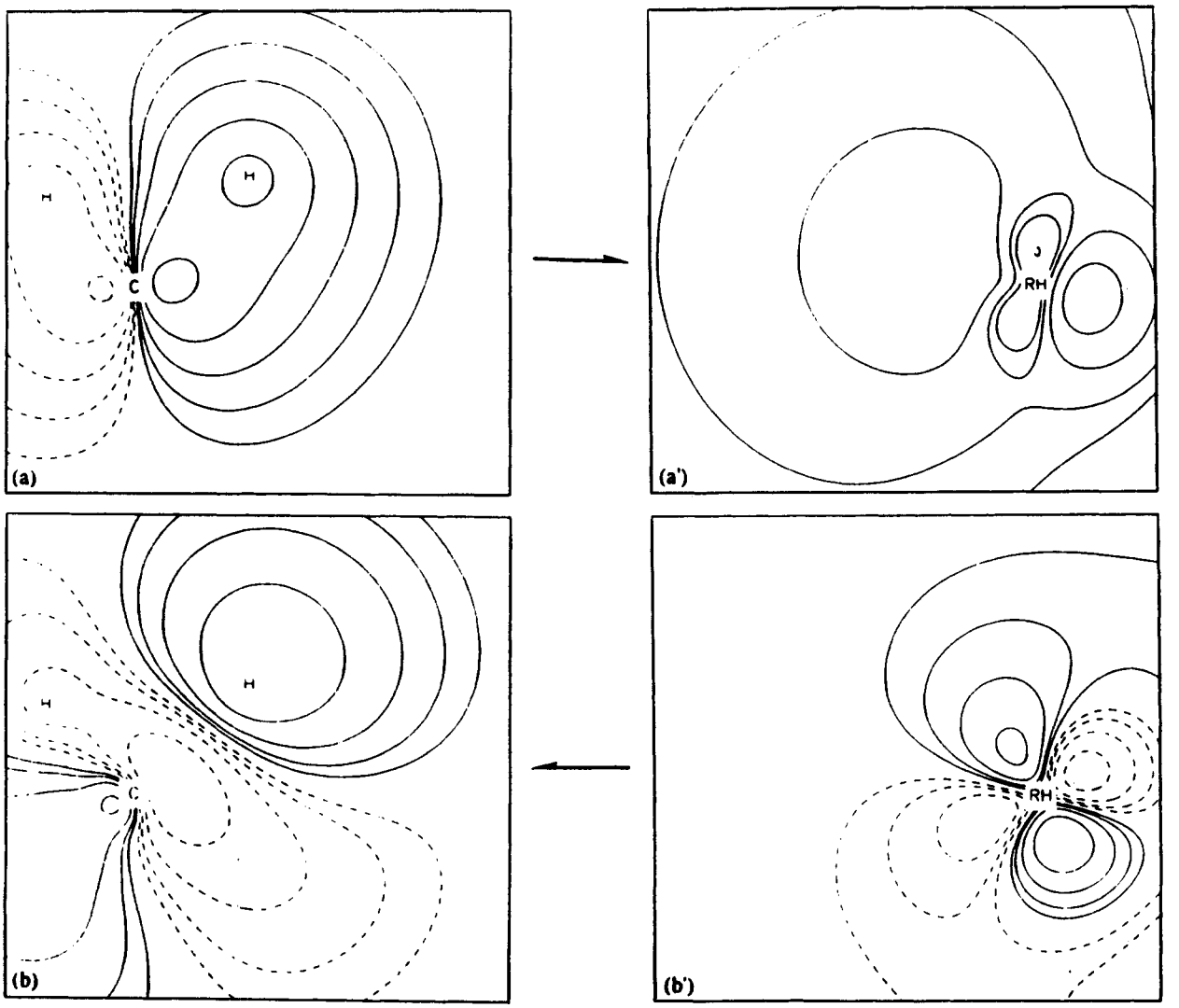

Figure 7. Contour plots for the frontier orbitals of the CH_4 and RhCpCO fragments in the transition state: (a) HOMO of the CH_4 fragment; (b) LUMO of the CH_4 fragment; (a') LUMO of the RhCpCO fragment; (b') HOMO of the RhCpCO fragment. The plots are in the Rh–H–C plane. The lowest contour values are 0.01563 (e Å^{-3})$^{1/2}$, and each succeeding contour differs from the previous one by a factor of 2.0. The arrows denote the directions of the electron donation.

"experimental" reaction coordinate with our theoretical one. To do this, we have used the definition of r_{bp}[25]

$$r_{bp} = [d_{MH}^2 + r^2 d_{CH}^2 - r(d_{MH}^2 + d_{CH}^2 - d_{MC}^2)]^{1/2} - r_{Rh} \quad (3)$$

where r is the ratio of the H covalent radius to the standard C–H distance[26] and r_{Rh} is the covalent radius of Rh. Figure 8 shows the variations in the Rh–H–C angle and d_{CH} with r_{bp}'s change. In the plots, we have omitted the first three points for large r_{bp} since our calculations are not sensitive enough to give reliable relative position of the Rh and C–H in the long-range region.

There are several important similarities between the "experimental" coordinate and our computed one. The experimental coordinate predicted an off-axis approach of the C–H bond at large r_{bp} (about 1.26 Å) with a Rh–H–C angle of 130°. Our theoretical coordinate gives a similar orientation, angle Rh–H–C = 125.7°, at r_{bp} = 1.08 Å, the largest value of r_{bp} in Figure 8. Our intermediate is located at r_{bp} = 0.70 Å corresponding to an agostic complex with moderately strong metal–CH interaction according to Crabtree et al.[25] Also, both the experimental reaction coordinate and our calculated one have predicted the rotation and elongation of the C–H bond as it approaches the metal. Since comparable systems are rare, the experimental coordinate has to stop at about r_{bp} = 0.5 Å, where the C–H bond has not yet shown an obvious lengthening. Thus, a transition state was estimated to be at about r_{bp} = 0.4 Å.[25] Strikingly, the position of the transition state predicted by our calculations is at r_{bp} = 0.37 Å.

There are also some differences between the experimental reaction coordinate and our theoretical one. The two curves in Figure 8 are roughly separated into two parts either side of the transition state. The rotation and elongation of the C–H bond in the late stage are more noticeable than that in the early stage. In other words, both rotation and lengthening of the C–H are accelerated in the transition state. However, the simultaneous acceleration is not present in the experimental coordinate. According to the experimental coordinate, before the C–H bond has been significantly lengthened, the M–H–C angle

(26) Since Crabtree used 0.28 as the value of r, where r is the ratio of the hydrogen covalent radius to the standard C–H distance, we also used 0.28 in this work for convenience of comparison. See ref 24 for additional explaination of the "experimental" reaction coordinate.

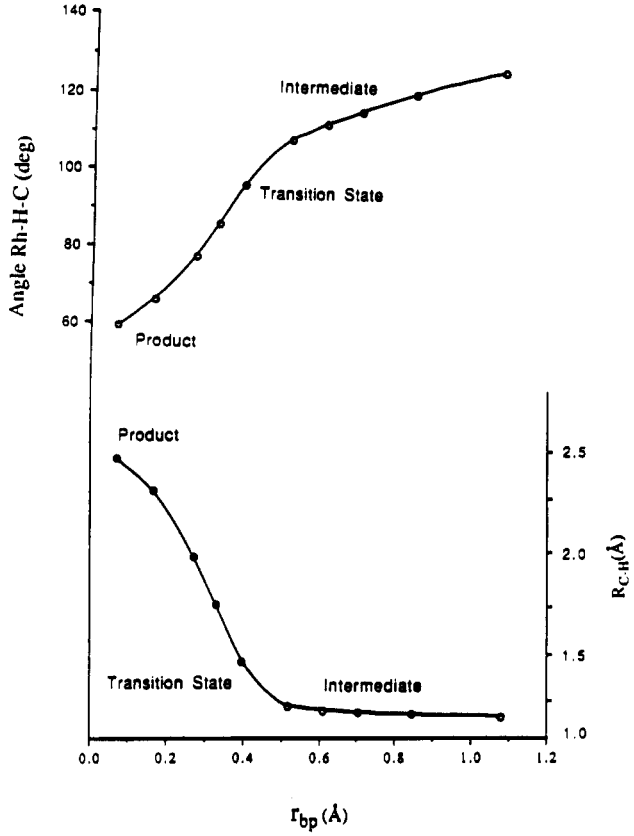

Figure 8. Variations of bond angle Rh–H–C and bond distance R_{C-H} along r_{bp}. The intermediate or transition state is denoted by ●.

falls rapidly. Thus, the experimental coordinate shows an obvious "pivoting motion".[7d,25] This implies that there is considerable steric interference before the reaction system enters the transition state. This kind of pivoting motion is less important according to our calculation, perhaps because we performed the calculations on the smallest alkane, methane, which should show smaller steric effect than the complexes used to construct the experimental coordinate. However, experimentally, "the successful alkane activation systems are all relatively unhindered".[7d] The solution to the problem of steric effects will need more detailed investigations both in experiment and theory.

F. Comparison with Previous Results. In a theoretical study using a density-functional method, Ziegler et al. investigated methane activation by the RhCp(CO) complex.[3h] The density-functional calculations predicted that the unsaturated 16-electron complex, RhCp(CO), has a singlet ground state with a X–Rh–C_o angle of 137°, where X is the center of the Cp ring and C_o is the carbon of the CO ligand. Our ab initio MO calculations gave a similar X–Rh–C_o angle, 137.2°, although the corresponding Rh–X and Rh–C_o distances are both longer than those obtained by the density-functional calculations.

Table III shows a comparison of the results from our ab initio RHF and MP2 calculations with the results from Ziegler et al. on the structure of the transition state and on the activation barrier. The transition-state geometry found by our calculations is much closer to the product than the transition state found by Ziegler et al.[3h] In addition, our calculations gave an activation barrier of 4.1 kcal/mol, which is close to the experimental value (4.5 kcal/mol).[8] From the density-functional theory the activation barrier is 8.8 kcal/mol and the transition state is even less stable than the reactants by 1.9 kcal/mol.

Table III. Comparison of the Activation Barrier for the Addition of CH_4 to RhCp(CO) and Important Geometric Parameters at the Transition State Obtained in Our and Other Studies

	E_{act} (kcal/mol)	R_{Rh-C} (Å)	R_{Rh-H} (Å)	R_{C-H} (Å)
Ziegler et al.[a]	8.8	2.53	1.74	1.56
this work	4.1	2.189	1.563	1.387
experiment[b]	4.5			

[a] Reference 3h. [b] Reference 8.

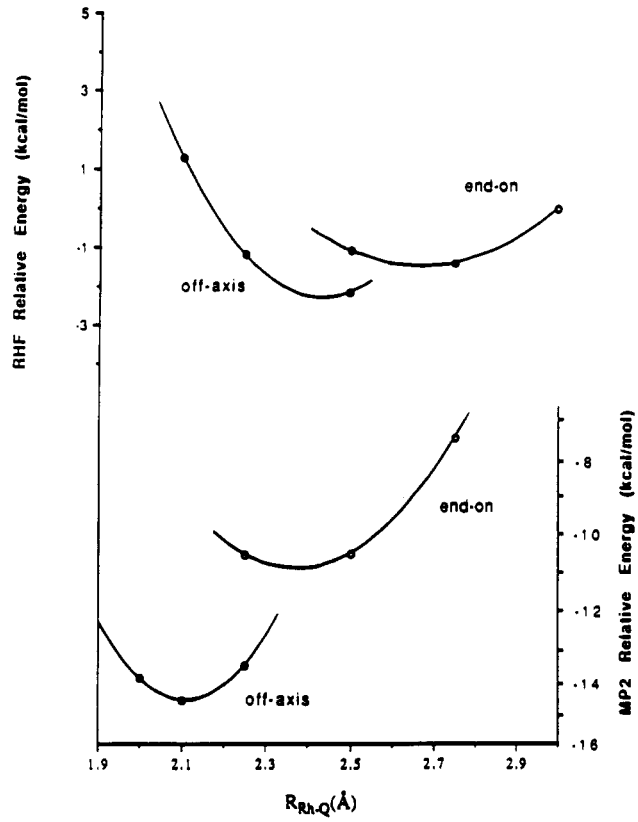

Figure 9. Potential energy curves for end-on and off-axis approaches along the coordinate R_{Rh-Q}.

Instead of optimizing the orientation of the C–H bond to get the intermediate, Ziegler et al. restricted the CH_4 to approach the metal in an end-on (M–H–C linear) fashion.[3h] The optimized end-on adduct was more stable than the reactants by 6.9 kcal/mol.[3h] To investigate the possibility of an end-on intermediate, we have performed additional calculations at both RHF and MP2 levels. In these calculations, the reaction system was restricted to an end-on geometry. The optimizations at RHF level were performed along the coordinate R_{Rh-Q}, which equals the sum of Rh–H distance and the half of the C–H distance. Then, MP2 calculations were carried out over the RHF optimized geometries. The energy curves for the end-on approach are compared with those for the off-axis approach (full optimization as shown in Figure 4) in Figure 9. The off-axis intermediate is obviously favored at the MP2 level, while it is only slightly favored at the RHF level. These results and the deformation density analysis for the intermediate (see Figure 6a) suggest that the interaction between the Rh and C atoms plays a significant role in determining the orientation of the C–H bond approaching the metal.

Conclusions

Methane C–H oxidative addition to RhCp(CO) has been investigated theoretically with ab initio RHF and MP2 techniques. Electron correlation has been found to be very important in describing the energetics of the reaction. At MP2 theoretical level, the calculated activation barrier is 4.1 kcal/mol and the exothermicity is 30.6 kcal/mol. In the early stage of the reaction, an intermediate has been predicted with a stabilization energy of 14.8 kcal/mol. These energetics are consistent with recent experimental results.[8]

The structural features of the intermediate suggest that it is an agostic-like complex with moderately strong metal–CH interaction. Furthermore, our analyses of the Laplacian of the charge density and deformation density indicate that the metal–CH interaction has dative-bond character. Obvious C–H bond breaking occurs in the transition state and leads to an increase of the energy. However, due to the additional formation of significant Rh–C and Rh–H interactions, the reaction system efficiently stabilizes the transition state. The calculated results also exhibit striking similarities with an "experimental" reaction coordinate but show smaller steric interference prior to the transition state.

Acknowledgment. The authors thank the National Science Foundation (Grant No. CHE 91-13634) and the Robert A. Welch Foundation (Grant No. A-648) for financial support and M. F. Guest for providing the GAMESS package of programs. This research was conducted in part using the Cornell National Supercomputer Facility, a resource of the Center for Theory and Simulation in Science and Engineering at Cornell University, which is funded in part by the National Science Foundation, New York State, and the IBM Corp. We also thank Cray Research for a grant of computer time on the CRAY Y-MP2/116 at the Supercomputer Center of Texas A&M University.

OM930319A